ACS APPLIED MATERIALS & INTERFACES

www.acsami.org Research Article

Hierarchical, Self-Assembled Metasurfaces via Exposure-Controlled Reflow of Block Copolymer-Derived Nanopatterns

Ashish A. Kulkarni and Gregory S. Doerk*

Cite This: *ACS Appl. Mater. Interfaces* 2022, 14, 27466−27475

Read Online

ACCESS | Metrics & More Article Recommendations Supporting Information

ABSTRACT: Nanopatterning for the fabrication of optical metasurfaces entails a need for high-resolution approaches like electron beam lithography that cannot be readily scaled beyond prototyping demonstrations. Block copolymer thin film self-assembly offers an attractive alternative for producing periodic nanopatterns across large areas, yet the pattern feature sizes are fixed by the polymer molecular weight and composition. Here, a general strategy is reported which overcomes the limitation of the fixed feature size by treating the copolymer thin film as a hierarchical resist, in which the nanoscale pattern motif is defined by self-assembly. Feature sizes can then be tuned by thermal reflow controlled locally by irradiative cross-linking or chemical alteration using lithographic ultraviolet light or electron beam exposure. Using blends of polystyrene-*block*-poly(methylmethacrylate) (PS-*b*-PMMA) with PS and PMMA homopolymers, we demonstrate both self-assembled PS grating and hexagonal hole patterns; exposure-controlled reflow is then used to reduce the hole diameter by as much as 50% or increase the PS grating linewidth by more than 180%. Transferring these nanopatterns, or their inverse obtained by a lift-off approach, into silicon yields structural colors that may be prescriptively controlled based on the nanoscale feature size. Furthermore, patterned exposure enables area-selective feature size control, yielding uniform structural color patterns across centimeter square areas. Electron beam lithography is also used to show that the lithographic resolution of this selective-area control can be extended to the nanoscale dimensions of the self-assembled features. The exposure-controlled reflow approach demonstrated here takes a pivotal step toward fabricating complex, hierarchical optical metasurfaces using scalable self-assembly methods.

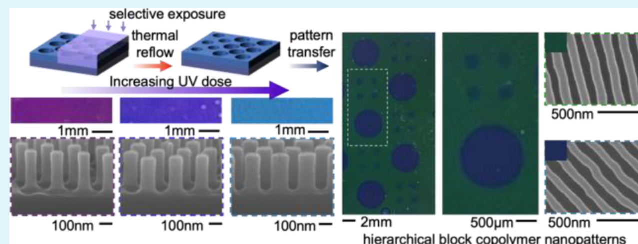

KEYWORDS: *block copolymers, self-assembly, optical metasurfaces, structural color, thermal reflow, solvent vapor annealing, lithography*

Downloaded via BROOKHAVEN NATL LABORATORY on November 23, 2022 at 18:05:57 (UTC).
See https://pubs.acs.org/sharingguidelines for options on how to legitimately share published articles.

■ INTRODUCTION

Optical metasurfaces consist of patterns with spatially varying nanoscale features, or "meta-atoms", that can be used to engineer novel optical functionality into materials by design. Many emerging optical metasurface applications such as polarization control, holography, and structural coloration require precise control of the size and placement of subwavelength patterns to manipulate light.[1−6] Because the resonant optical responses in the meta-atoms that underpin the functional properties of metasurfaces are often dictated by their feature size,[3,7,8] nanopatterning methods for metasurface fabrication must achieve both broad tunability and precise control over feature sizes of local patterns. So far, this has been achieved using electron beam,[2,3] deep ultraviolet,[9,10] or nanoimprint lithography,[7] whereby predefined nanoscale patterns are precisely written in a patternable "resist" layer, followed by pattern transfer to form metallic or dielectric meta-atoms. Electron beam lithography has been a workhorse tool for metasurface prototyping based on its patterning flexibility and high resolution, but the serial exposure process renders its throughput too low for mass production. On the other hand, deep ultraviolet lithography is a proven patterning technology for nanoelectronics, but high system costs and limited resolution may impose practical limits on its use for metasurface fabrication.[11] Nanoimprint lithography has emerged as a scalable nanopatterning approach for metasurface fabrication.[12,13] The prerequisite for templates at the resolution of the metasurface design, however, renders nanoimprint lithography economical for high production volumes (e.g., >10^5 300 mm wafers),[14] limiting the potential for customized metasurface designs. Clearly, new nanopatterning methods are critical to translating optical metasurfaces from prototyping to production.

Self-assembly, the spontaneous self-organization of nanoscale components, has been proposed as a scalable and cost-effective alternative to traditional nanolithography for metasurface fabrication.[15−18] For instance, the self-assembly of block-copolymer thin films generates various uniform nanoscale patterns, including line/space gratings and dots/holes, with

Received: April 4, 2022
Accepted: May 20, 2022
Published: June 3, 2022

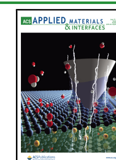

© 2022 American Chemical Society

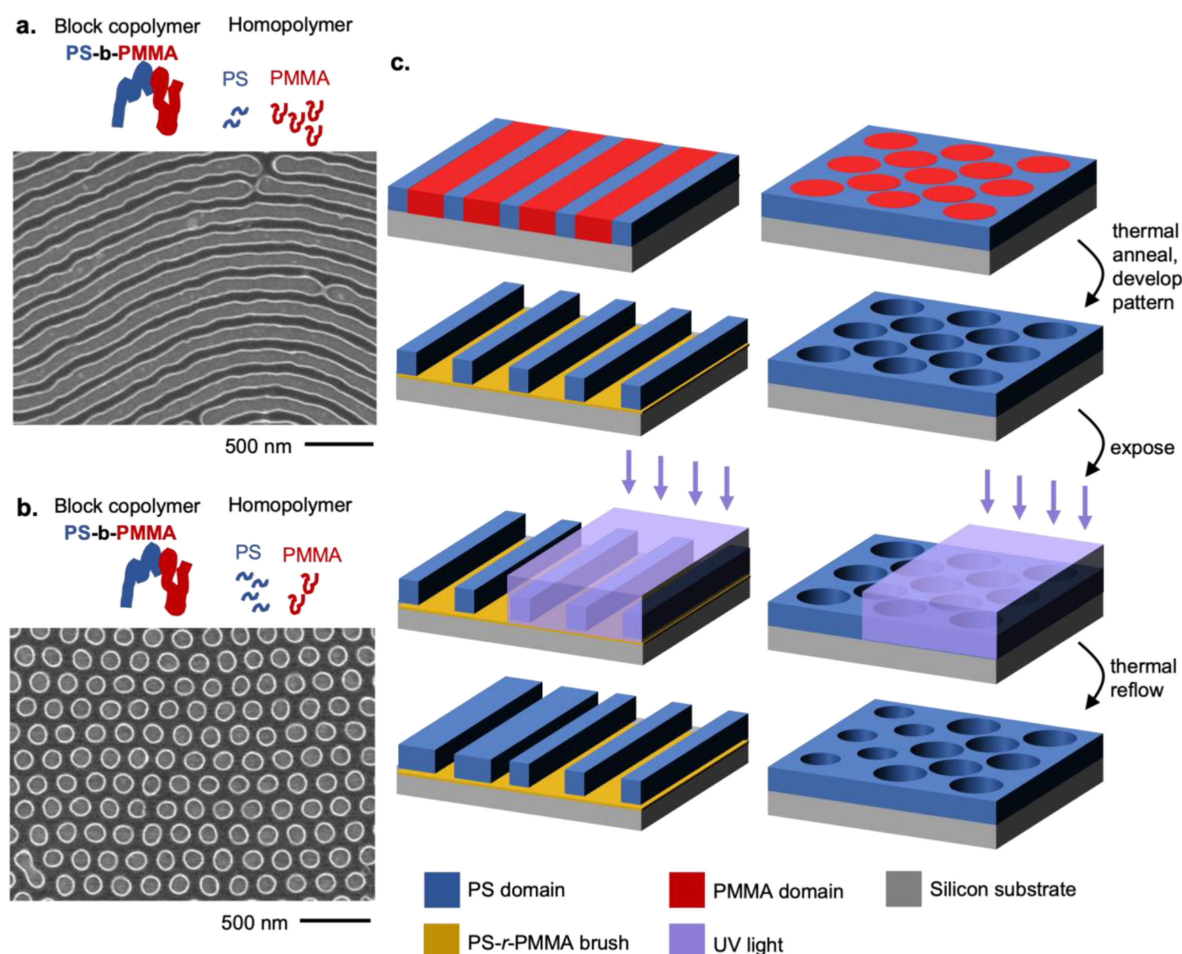

Figure 1. Schematic for hierarchical photopatterning. SEM images of (a) grating and (b) hole nanopatterns after PMMA development, obtained through self-assembly of PS-*b*-PMMA (40% w/w) blended with PS and PMMA homopolymers in different mass ratios. Remnant PS features appear dark. The process flow schematic (c) shows the steps involving a brief thermal anneal and pattern development for the block copolymer blends with a homopolymer after solvent vapor annealing. UV exposure is then used to partially cross-link the PS, limiting the extent of reflow for exposed regions in a subsequent, brief thermal treatment.

fixed symmetry, period, and domain size across an entire substrate, as dictated by the block copolymer molar mass and the volume fraction of the blocks. Notably, self-assembled block copolymer nanopatterns have been scaled to large areas as part of continuous[19] or batch[20] manufacturing processes. However, self-assembly methods using block copolymers and other materials generally lack the flexibility in local definition of meta-atom size, shape, and spacing afforded by conventional lithography. To enable hierarchical nanopatterning, a degree of localized control over the self-assembled block copolymer nanopattern type, spacing, and domain size has been achieved through directed self-assembly using nanoscale templates,[21−23] irradiative chemical alteration and reassembly,[24−29] or electrohydrodynamic jet printing.[30] Nevertheless, these strategies offer modest feature size tunability, require high resolution nanoscale lithographic directing templates, or depend on specialized tools and reaction chambers. As a result, they may diminish much of the intended benefit of using self-assembled nanopatterns.

Here, we introduce a versatile strategy for creating hierarchical nanopatterns through exposure-controlled thermal reflow. In this strategy, a block copolymer thin film is used as a kind of hierarchical resist, in which an initial nanoscale pattern motif is defined via self-assembly. Nanopattern feature sizes are then tuned locally by irradiation-induced cross-linking or chemical alteration and subsequent thermal reflow of the polymer. Using patterns formed by PS-*b*-PMMA blended with PS and PMMA homopolymers, we demonstrate both a tunable reduction in the diameter of hexagonally arranged nanoscale holes in PS by as much as 50% and a tunable increase in the linewidth of PS grating nanopatterns by more than 180%. Moreover, we show that lithography processes such as shadow-masking and electron beam writing enable prescriptive, hierarchical modification of the nanopatterns across several orders of magnitude, from nanoscale writing (<100 nm) to macroscale printing (>1 mm). Locally defined structural colors generated by etching these hierarchical nanopatterns into underlying silicon (Si) substrates illustrate the viability of this technique for fabricating more complex optical metasurface devices.

■ RESULTS AND DISCUSSION

Following the methods described in ref 31, self-assembled polymer thin films of PS-*b*-PMMA (536-*b*-515 kg mol^{-1}) blended with PS (3.5 kg mol^{-1}) and PMMA (3 kg mol^{-1}) homopolymers were obtained on a Si substrate with a previously grafted PS-*r*-PMMA random copolymer brush by spin casting and solvent vapor annealing (see Figure S1,

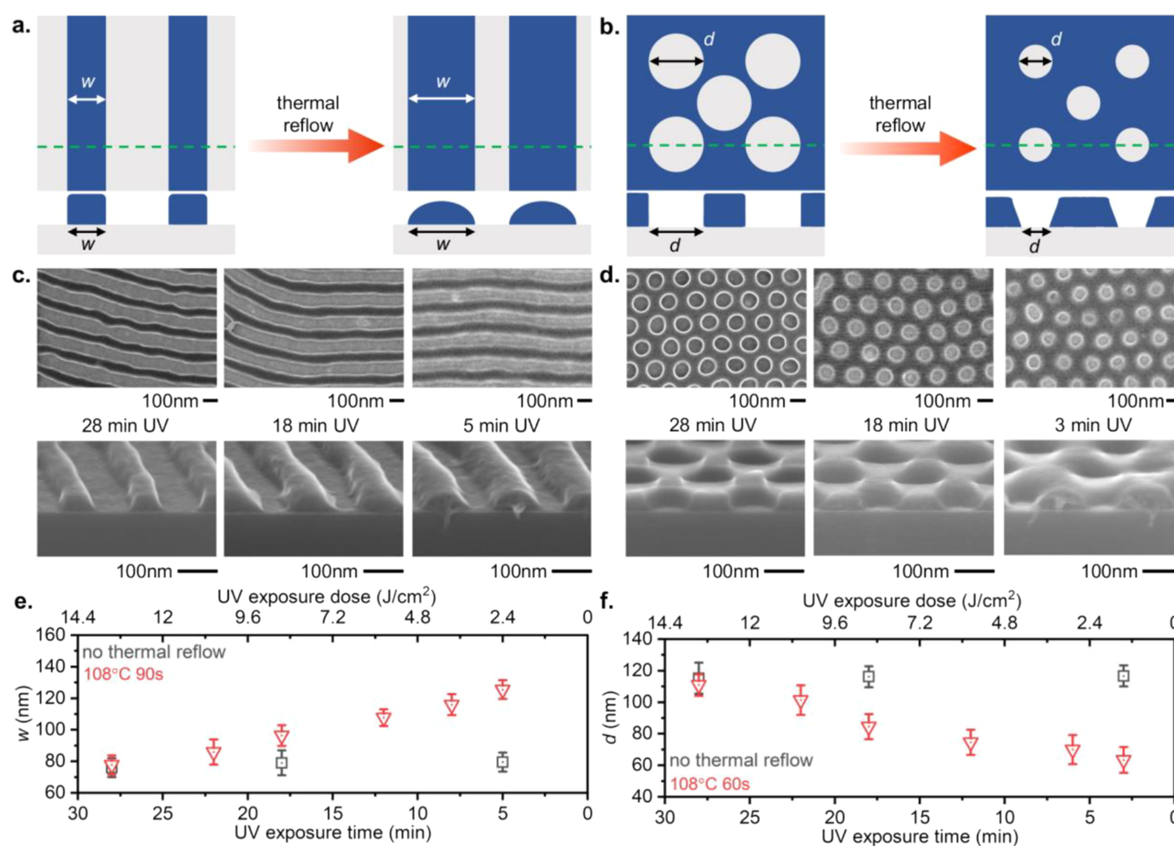

Figure 2. Feature size is tuned by UV exposure and thermal reflow. Schematics in (a) and (b) depict the tunable variations in the feature sizes for each blend morphology, based on the UV exposure dose and thermal reflow conditions. The linewidth, *w*, in gratings is defined in (a), while the hole diameter, *d*, is defined in (b). SEM images in (c) and (d) show the plan-view (top row) and cross-sectional view (bottom row) of the grating and hole patterns, respectively, corresponding to the denoted UV exposure times after thermal reflow at 108 °C for 90 and 60 s, respectively. The plot in (e) shows the change in the grating linewidth, *w*, while the plot in (f) shows the change in hole diameter, *d*, with respect to the extent of UV exposure at a constant thermal reflow condition. Error bars in (e) and (f) show one standard deviation.

Supporting Information). The solvent vapor annealed films were then subjected to a brief step of thermal annealing to sharpen the self-assembled domain interfaces.[31] Subsequently, the samples were exposed to ultraviolet (UV) light in a chamber continuously purged by nitrogen and then immersed in acetic acid to etch away the PMMA components (see Methods for details). By decreasing the ratio of PMMA to PS homopolymer, the self-assembled morphology of the blend can be shifted from forming nanopattern "gratings" (i.e., lines and spaces) to "holes," as shown by the scanning electron microscopy (SEM) images in Figure 1a,b, respectively. After development, the remnant PS features of the grating pattern exhibit a period of 182 ± 2 nm (see Figure S2, Supporting Information) and average linewidth, *w* of 79 ± 7 nm, while holes exhibit a period of 213 ± 2 nm (see Figure S2, Supporting Information) and average diameter, *d* of 116 ± 7 nm. We note that the highly ordered domain periods larger than 100 nm achieved using ultrahigh-molecular-weight block copolymers[32,33] provide flexibility for fabricating metasurfaces with responses at visible wavelengths or longer using high-refractive index materials like Si. This is in stark contrast to patterns that are possible using lower molecular weight block copolymers, whose sub-50 nm critical dimensions limit their use to plasmonic and deep sub-wavelength applications.[34−37]

The process flow for selectively tuning the size of either the lines or holes by exposure-controlled reflow is depicted schematically in Figure 1c. After selective PMMA removal, the size of the remnant PS features can be modified by thermal reflow to an extent controlled by exposure-induced PS cross-linking via UV irradiation in the same nitrogen-purged chamber. UV-induced cross-linking of PS is well established.[38−45] In particular, in vacuum or an environment with no or low oxygen content, absorption of UV light at an ∼254 nm wavelength produces polymer macroradicals by hydrogen abstraction that may subsequently cross-link.[43−45] To confirm PS cross-linking, we measured the swelling of ∼200 nm thick, 22 kg/mol PS thin films in a saturated vapor of tetrahydrofuran (a good solvent for PS) as a function of UV exposure time up to 70 min. A decrease in swelling is observed for increasing exposure time (see Figure S3, Supporting Information), indicating a gradual increase in the cross-linking density.[46] Meanwhile, the mean water contact angle measured for PS films exposed for 0 to 70 min, sampled at 14 min exposure intervals, is 91 ± 2° (3 × standard deviation), which indicates a negligible degree of surface photo-oxidation.[47,48] This gradual cross-linking with longer exposure reduces polymer mobility, thus decreasing the rate of feature size change by reflow. Although the brief UV exposure (3−5 min) prior to the pattern development is sufficient to remove all PMMA,[49] the extent of PS cross-linking in this time period is minimal; additional exposure to UV light may therefore be used to further cross-link PS.

By controlling the UV exposure dosage and thermal reflow conditions, the linewidth, *w* (defined in Figure 2a), in grating

https://doi.org/10.1021/acsami.2c05911
ACS Appl. Mater. Interfaces 2022, 14, 27466−27475

nanopatterns can be increased, while the hole diameter, d (defined in Figure 2b), can be decreased. As observed in the SEM images (see various panels in Figure 2c,d), the cross-sectional profiles of the PS features change after reflow to an extent that depends explicitly on the previous time (or dose) of UV irradiation (after reflow at 108 °C for 90 and 60 s, respectively). Indeed, plots in Figure 2e,f show that for a fixed thermal reflow time and temperature, the feature size depends on the UV dose in a nominally linear fashion. It should be noted that feature heights necessarily decrease as lateral feature sizes change upon reflow due to volume conservation. Indeed, the average PS grating height measured from cross-sectional SEM images in Figure 2c reveals a line height reduction of ∼10 nm as UV exposure time is reduced from 28 to 5 min, which has potential implications for pattern transfer.

By reducing polymer mobility, UV-induced cross-linking changes the rate, not the extent, to which feature sizes change during polymer reflow. As a phenomenon that is highly sensitive to temperature (above the glass transition) and time, significant adjustments in nanopattern feature sizes are possible through judicious selection of these process parameters. For instance, by increasing the reflow temperature to 112 °C, grating linewidths can be increased from 79 ± 7 nm to 150 ± 6 nm (a ∼90% increase, see Figure S4, Supporting Information), while the diameters in hole nanopatterns can be reduced from 116 ± 7 nm to 57 ± 8 nm (a ∼ 50% reduction, see Figure S4, Supporting Information). Increasing reflow time can also be used to augment the feature size, though extended durations of reflow will ultimately form a homogeneous PS layer. Additionally, by varying the PS homopolymer fraction in the initial composition for the grating pattern-forming blends, the range of linewidths can be further expanded. For instance, in a film composed of 40% 1051 kg mol^{-1} PS-*b*-PMMA blended with 60% PMMA 3 kg mol^{-1} homopolymer, the PS linewidth in the developed pattern is 52 ± 7 nm. By controlling the UV exposure time and thermal reflow conditions, that linewidth can be increased to 150 ± 6 nm, enabling feature size tunability by more than 180% (see Figure S5, Supporting Information). We note that the UV exposure process does not result in any change in the feature sizes unless a subsequent thermal reflow step is performed (see Figure 2e,f and S4 and S6, Supporting Information), as expected. Moreover, if the initial UV exposure step is not performed prior to developing the PMMA components, UV exposure-controlled thermal reflow can still be carried out on the remnant polymer. However, the obtained patterns exhibit uneven features (see Figure S7, Supporting Information). Finally, analysis of Fourier transforms of SEMs (taken after pattern transfer, discussed below) verifies that the pattern spacing remains effectively invariant, while the average sizes of pattern features are augmented through polymer reflow (see Figures S8 and S9, Supporting Information).

A key prerequisite for any effective resist is high fidelity transfer of the patterned features into other functional materials. Here, we demonstrate that the size-tunable features in our self-assembled hierarchical resist can be transferred readily by dry etching into Si, a high-refractive index, CMOS compatible material that has found wide use in metasurface-based devices.[50] PS exhibits a reasonably good dry etch resistance in comparison to other organic polymers used in nanopatterning like PMMA[51,52] and may therefore be used directly as an etch mask for reactive ion etching (RIE; see Methods for details). The PS grating nanopattern was transferred into Si following this approach, resulting in ∼180 nm deep trenches (see Figure 3a,b). PS patterns may also be

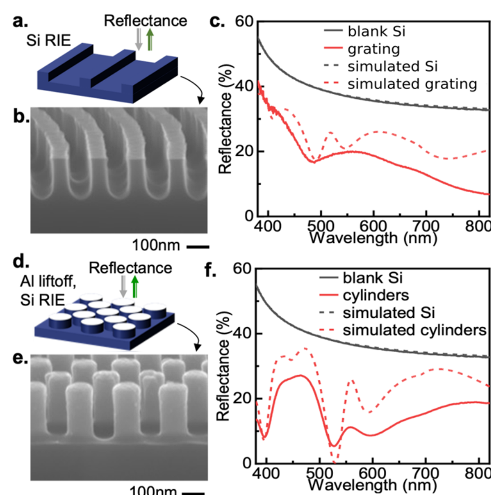

Figure 3. Structural color response. (a) Schematic and (b) cross-sectional SEM image showing a representative grating pattern transferred into Si via RIE using PS features as an etch mask. (c) Measured (solid line) and simulated (dashed line) normal-incidence reflectance for the sample shown in (b). (d) Schematic and (e) cross-sectional SEM image showing a representative cylinder pattern transferred into Si via RIE using Al liftoff metal as an etch mask. (f) Measured (solid line) and simulated (dashed line) normal-incidence reflectance for the sample shown in (e).

inverted using material deposition and a subsequent liftoff process (see Figure S10, Supporting Information). This approach was applied using aluminum (Al) to invert the hole patterns, wherein subsequent RIE using the Al liftoff mask results in ∼220 nm tall cylindrical pillars (see Figure 3d,e).

These Si grating and pillar arrays exhibit distinctive optical responses, as shown by specular reflectance spectra (solid curves) taken from these samples in Figure 3c,f, respectively. These phenomena can be attributed to Mie-scattering-mediated electromagnetic resonances in the Si meta-atoms with subwavelength feature sizes, which when coupled to the underlying Si substrate give rise to wavelength-dependent dips in the reflection spectra.[53] Finite-difference time-domain (FDTD) optical simulations were performed to corroborate this hypothesis (dashed curves in Figure 3c,f; see Methods for details). The two distinctive dips that appear in the wavelength range of 450−650 nm in the simulated reflectance spectra for both gratings and pillars play a key role in their structural color response. The simulated dip positions agree particularly well with those measured experimentally from the Si nanopillars (Figure 3f). Comparison with previous investigations of Mie resonances from Si nanopillars indicates that the lower wavelength dip in the vicinity of ∼530 nm can be attributed to a magnetic dipole resonance in Si nanopillars on a Si substrate.[8,53] The higher wavelength dip arises because of strong field enhancements in the narrow air gap between high-refractive index pillars when their spacing is reduced to less than ∼225 nm.[8]

The self-assembled nanopatterns modified by UV exposure and thermal reflow can also be transferred into the underlying Si substrate, enabling a tunable optical response witnessed by changes in structural coloration. For instance, the diameter of the etched Si nanopillars can be prescriptively adjusted by

https://doi.org/10.1021/acsami.2c05911
ACS Appl. Mater. Interfaces 2022, 14, 27466−27475

exposure-controlled thermal reflow prior to PS hole pattern inversion and Si etching. Here, we demonstrate diameter tunability from ∼110 (28 min UV exposure) to ∼95 nm (3 min UV exposure) after reflow at 104 °C for 60 s, Al lift-off, and RIE (∼270 nm deep), as shown in Figure 4a,b. These changes in the cylinder diameter change the emergent structural color from cyan to magenta (Figure 4c) as a result of shifts in the position of a reflectance dip in the wavelength range of ∼560 to 620 nm that we can ascribe to Mie-type resonances (Figure 4d). As noted earlier, FDTD simulations (Figure 4e) predict two reflectance dips in the range of ∼500 to 620 nm. The dotted lines in Figure 4d,e indicate that the higher wavelength resonance mode is more strongly dispersive and therefore plays a prominent role in the structural color response.

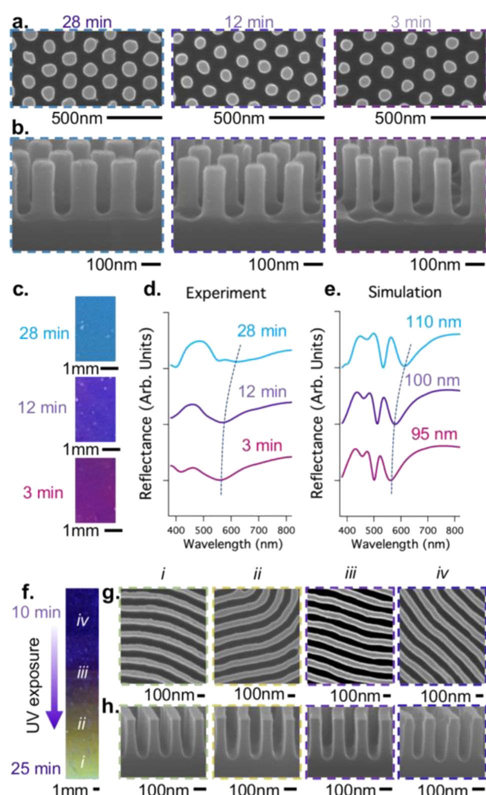

Figure 4. Exposure-tuned structural color. (a) Plan-view and (b) cross-sectional SEM images of etched cylinder patterns, which were subjected to UV exposure of 28, 12, and 3 min, and thermal reflow at 104 °C for 60 s. Photographs in (c) show the macroscopic color response from etched patterns in (a) and (b). (d) Measured and (e) simulated reflectance spectra from the samples shown in (c). (f) is a photograph showing the range of colors obtained from etched grating patterns, which were subjected to a gradual variation in UV exposure, from 25 to 10 min, in steps of 1 min and thermal reflow at 112 °C for 90 s. (g) Plan-view and (h) cross-sectional SEM images taken at positions *i* through *iv* depicted in (f).

The experimental resonances of these two modes are broad and overlap, in contrast to the FDTD simulations based on idealized structures. This can be ascribed to the presence of defects and natural variations in the position, size, and lattice orientation of features in “fingerprint” patterns obtained via undirected self-assembly, which lack a long-range order or unidirectional alignment.[54] Roughness observed in Si nanoscale structures transferred from these fingerprint patterns may also contribute to spectral broadening, especially when the roughness yields substantial variability and inhomogeneity in the Si nanostructure dimensions. These variations may pose a challenge to using self-assembled patterns for structural color. However, dramatic improvements in the quality of the optical response can be expected by extending our technique to block copolymer patterns previously defined by directed self-assembly,[55,56] which exhibit minimal pattern defectivity, prescribed lattice orientation, low roughness, and exquisite pattern feature uniformity.[57,58] The narrow pillar spacings made possible using self-assembled patterns as shown here offer additional avenues for improving color saturation through the coupling of Mie resonances and lattice resonances using judiciously selected substrates.[59,60]

Like the cylindrical nanopillar diameter, the Si grating linewidth can be adjusted by controlled exposure and reflow of the self-assembled PS resist grating pattern. To demonstrate this tunability, we exposed PS grating patterns with 10 to 25 min of UV in steps of 1 min across a single sample, followed by thermal reflow at 112 °C for 90 s, to generate line/space patterns with a macroscopic gradient in the PS linewidth. Subsequent RIE (∼320 nm deep) transferred the varying linewidth patterns into Si, giving rise to a range of colors from green and yellow to violet as shown in Figure 4f. Scanning electron micrographs (Figure 4g,h) reveal that these color changes correlate with increasing Si linewidth from 70 to ∼100 nm from points *i*−*iv* with decreasing UV dose, which in turn red-shifts the positions of the reflectance dips (see Figure S11, Supporting Information). Despite the curved cross-section profile of the wider PS features after reflow (Figure 2c), the transferred Si gratings maintain a steep vertical profile across the entire range of PS linewidths, helping to ensure color purity.

Varying the exposure doses of UV radiation in selected areas can be used to impart localized differences in the extent of cross-linking of the PS patterns. Upon thermal reflow, the dose locally applied to these exposed regions dictates the ultimate feature size, resulting in hierarchical patterns, in which the nanopattern motif is determined through self-assembly, but the feature size is set by the exposure pattern. For instance, in Figure 5a we show a hierarchical grating nanopattern in which circular regions were exposed to UV for 28 min, while the surrounding field was exposed to UV for 8 min, using a shadow mask. After thermal reflow (at 108 °C for 90 s) and RIE (∼205 nm deep) onto the underlying Si substrate, the Si gratings in the circular regions possess an average linewidth of ∼70 nm, while those in the surrounding field possess an average linewidth of ∼100 nm (see Figure 5b,c). These differences in the linewidth give rise to a macroscopic colored pattern with blue circles in a green field. Acknowledging the modal broadening and overlap noted earlier, the shapes of the experimental reflectance spectra (Figure 5d) agree well with the corresponding spectra simulated using FDTD calculations at the same linewidths (Figure 5e), underscoring the importance of nanoscale structural electromagnetic resonances in producing the localized color difference. A difference in height less than 20 nm between Si gratings in the circular regions and the field, as measured from the cross-sectional SEM images (Figure 5c), may also contribute to the differential structural color response. FDTD calculations with height varying from 180 to 205 nm at a fixed 70 nm Si grating linewidth reveal an expected position shift of the resonance in the vicinity of the ∼540 nm wavelength by approximately 10−

https://doi.org/10.1021/acsami.2c05911
ACS Appl. Mater. Interfaces 2022, 14, 27466−27475

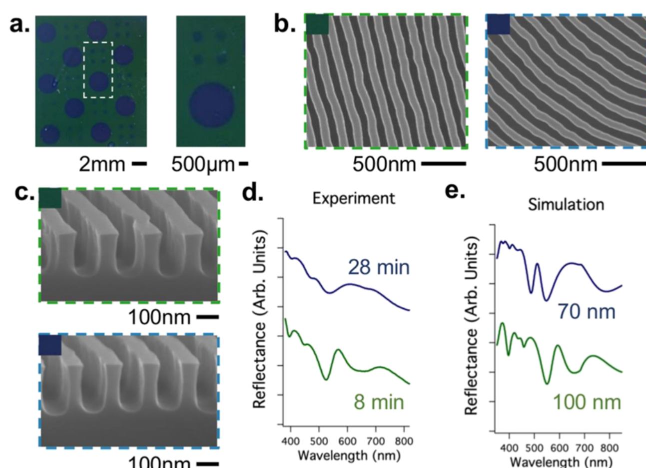

Figure 5. Hierarchical photopatterning by shadow mask lithography. (a) Photograph of a two-color macro-pattern obtained from gratings exposed to UV through a shadow mask and transferred into Si. The magnified image shows the white dotted region. (b) Plan-view and (c) cross-sectional SEM images show the transferred patterns from the regions showing the green and blue color. The sample was initially subjected to 8 min of UV exposure with an additional 20 min of UV exposure through the shadow mask followed by thermal reflow at 108 °C for 90 s. The PS lines were used as an etch mask for pattern transfer into Si by RIE. (d) Measured and (e) simulated reflectance spectra from the two-color regions with the given linewidths.

20 nm, with no major change in overall reflectance spectra shapes, indicating that the effect of this small height difference on the structural color is modest in comparison to the effect induced by changes in the linewidth (see Figure S12, Supporting Information).

It is worthwhile to note that the circle-to-circle color consistency and the overall color uniformity across the entire pattern area show that this hierarchical patterning method can provide consistent nanopattern control across at least centimeter scale areas. Furthermore, although the smallest shadow mask feature we demonstrate here is ~500 μm, the selective pattern size and shapes are ultimately limited by the mask design and exposure method, similar to conventional resists. Hierarchical nanopatterns, in which a fixed pattern motif is maintained everywhere but feature sizes vary locally by design, have been the hallmark of many structural color displays and optically resonant metasurfaces more generally.[61] The ability to replicate this using self-assembled nanopatterns, as demonstrated here, will engender new opportunities for low-cost manufacturing of metasurfaces across large areas.

Next, we demonstrate that by using electron beam lithography, hierarchical patterning via exposure-controlled reflow can be extended to nanoscale resolution. Figure 6a,b shows a sample hierarchical pattern achieved through electron beam exposure of a hole nanopattern after thermal reflow at 107 °C for 60s. Surprisingly, the hole diameter is smaller in the exposed regions (darker), indicating faster reflow that is in direct contradiction to the prior results in the present report obtained from UV exposure. This behavior is also observed in the grating nanopatterns, as shown in Figure 6c−e, which present rectangular electron beam exposure patterns after thermal reflow 107 °C for 90s with lengths of 500 nm and widths of 2 μm, 500 nm, and 50 nm, respectively. In the last instance (Figure 6e), the exposed width is smaller than the self-assembled feature linewidth, suggesting prospects for creating

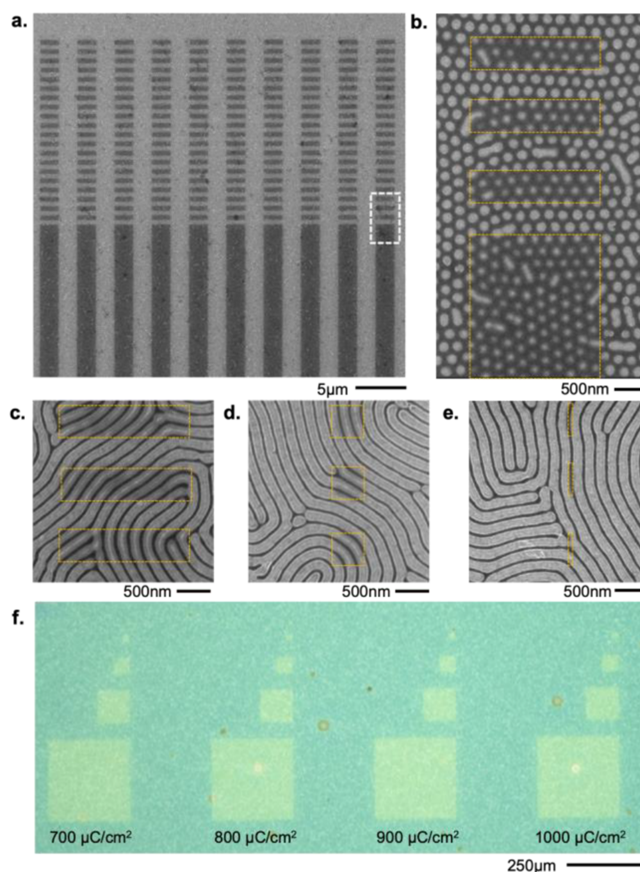

Figure 6. Hierarchical patterning by electron-beam exposure. SEM images of localized electron beam exposure patterns by electron beam lithography of (a−b) self-assembled hole nanopatterns followed by thermal reflow at 107 °C for 60 s (with inset area (b) marked by a dotted white box in (a)), and (c−e) self-assembled grating nanopatterns followed by thermal reflow at 107 °C for 90s. Dotted yellow lines demarcate areas of electron beam exposure in (b−e). (f) An optical microscope image of electron beam-exposed square arrays of grating nanopatterns after thermal reflow at 106 °C for 90 s and pattern transfer into Si by RIE. The exposure dose varies from 700−1000 μC/cm^2 across the square arrays in 100 μC/cm^2 increments (from left to right) per array.

metasurfaces with sculpted nanoscale features by self-assembly through this hierarchical resist concept. These results further confirm that the resolution of our hierarchical nanopatterning approach is ultimately limited by the exposure method.

Electron beam-exposed grating nanopatterns after thermal reflow (106 °C for 90s) and pattern transfer into Si exhibit an altered optical response, as shown by an optical microscope image of electron beam-exposed square arrays (Figure 6f) with square lengths of 250, 100, 50, 20, 10, 5, and 1 μm (squares smaller than 10 μm could not be resolved at this magnification). The squares exhibit a clear color difference with the background. However, there is no obvious dependence on the electron dose, which varies from left to right across the arrays from 700 to 1000 μC/cm^2 in 100 μC/cm^2 increments. This is despite the fact that the reflow is indeed sensitive to the exposure dose (see Figure S13, Supporting Information).

The apparent enhancement in reflow for PS exposed to an electron beam can be attributed to chemical changes that occur in PS under electron irradiation. PS has been used previously as a negative tone electron beam resist,[62] where cross-linking

https://doi.org/10.1021/acsami.2c05911
ACS Appl. Mater. Interfaces 2022, 14, 27466−27475

behavior was surmised from the insolubility in organic solvents with sufficient exposure dose. However, photoluminescence[63] and Raman spectroscopic[64] characterization studies of electron-irradiated polystyrene indicate the formation of polycyclic aromatic hydrocarbons and disordered amorphous carbons, respectively. Such hydrocarbons may leach out upon heating. We hypothesize that a hydrocarbon layer coats the surface between PS features upon reflow, affecting the etch depth in subsequent pattern transfer but minimally altering the feature size. As a result, the exposed regions exhibit an altered structural color based on the shorter height of Si nanostructures after pattern transfer in the electron beam-exposed regions compared to the height of nanostructures in the surrounding unexposed areas. This assessment is supported by the negligible color change in the exposed regions with varying electron exposure dose, even across larger and smaller doses and for lower electron beam accelerating voltages. PS-*b*-PMMA is therefore not an optimal hierarchical resist when using electron beam lithography; other block copolymers, however, would likely meet the necessary requirements. For instance, block copolymers containing polydimethylsiloxane (PDMS) may be ideal candidates given the high electron cross-linking yield for PDMS, which is 50−100 times that of PS.[25]

■ CONCLUSIONS

In summary, we have reported a new and versatile method to locally control the feature sizes of self-assembled nanopatterns using simple lithography tools through exposure-controlled polymer reflow. By applying our method to thin film nanopatterns formed by blends with ultrahigh-molecular-weight block copolymers, we demonstrate hierarchical patterning with locally defined reflective structural color. The facile transferability of these self-assembled patterns, even without a long-range order, highlights their strong potential for the fabrication of high-quality optical metasurfaces.[16,17,65−67] We envision applying this approach to other block copolymer chemistries or combining it with nonetching pattern transfer techniques[68,69] to fabricate metasurfaces featuring a variety of metal or metal oxides. Moreover, applying this method to block copolymer patterns previously defined by directed self-assembly will dramatically reduce pattern defectivity and improve pattern feature uniformity[57,58] while imposing the wafer-scale pattern order and alignment required for metasurface-based light polarization and phase manipulation applications. The self-assembled, hierarchical resist approach presented here has the potential to promote widespread adoption of nanophotonics, for example, by lowering the resolution requirements for roll-to-roll photolithography[70] or by simplifying the fabrication of master templates for nanoimprint lithography.

■ EXPERIMENTAL SECTION

Materials. The nearly symmetric 1051 kg mol^{-1} PS-*b*-PMMA (M_n = 536−515 kg mol^{-1}, PDI = 1.10; T_g = 107 °C/132 °C) block copolymer, and PS (M_n = 3.5 kg mol^{-1}, PDI = 1.05; T_g = 77 °C)[54] and PMMA (M_n = 3 kg mol^{-1}, PDI = 1.14; T_g = 74 °C)[54] homopolymers were obtained from Polymer Source Inc. and used as received. These polymers were dissolved in propylene glycol monomethyl ether acetate (PGMEA) at a concentration of 2% by weight. The grating nanopattern was obtained from blending the PS-*b*-PMMA block copolymer with PS and PMMA homopolymers in mass fractions of either 40, 20, and 40%, respectively, or 40% block copolymer with 60% PMMA homopolymer. The hole nanopattern was obtained from blending the PS-*b*-PMMA block copolymer with PS and PMMA homopolymers in mass fractions of 40, 40, and 20%, respectively. For cross-linking studies, PS (M_n = 22.0 kg mol^{-1}, PDI = 1.1) was dissolved in toluene at a concentration of 5% by weight.

Sample Preparation. Si wafers were first cleaned with O_2 plasma (for 120 s at 21 W, 100 mTorr) using a March Plasma CS1701 reactive ion etching tool. These cleaned substrates were then coated at 1500 rpm with a thin film of PS-*r*-PMMA-OH random copolymer "brush" (60 mol % styrene; Dow Chemicals) dissolved in PGMEA (1% w/w) and baked on a preheated hot plate at 250 °C for 5 min in air to graft a monolayer brush to the substrate. The ungrafted brush was removed by spin-rinsing in PGMEA at 3000 rpm. The substrates were then spin-coated with the block copolymer−homopolymer blend solution at 1500 rpm, resulting in a film thickness of ∼80 nm. These films were then subjected to solvent vapor annealing performed using tetrahydrofuran with nitrogen purging at a controlled flow rate of 0.5−0.8 sccm. The swollen film thickness was constantly monitored as described in ref 31 during solvent vapor annealing for 60 min to achieve a maximum swell ratio of ∼3.6 (polymer fraction ϕ = 0.28) and ∼ 3.4 (polymer fraction ϕ = 0.29) for blends producing grating and hole nanopatterns, respectively (see Figure S1, Supporting Information). Without a random copolymer brush, hole nanopatterns will not form (as cylindrical domains do not orient vertically) and the polymer film is more likely to dewet. After 60 min, the annealing process was quenched, resulting in complete drying of the film in ∼1 s. After solvent vapor annealing, the samples were thermally annealed on a preheated hotplate at 250 °C for 30 s to achieve a sharp interface between the PS and PMMA features.[31] Furthermore, the samples were placed into a chamber isolating them from room light and exposed to ultraviolet light generated from a low-pressure 17 W mercury lamp (G10T5 1/2VH, Atlantic Ultraviolet Corporation) for 3−5 min under constant nitrogen purging followed by immersion in acetic acid for 3 min to remove PMMA and rinsing with deionized water. This UV exposure with an optical power of about 8 mW cm^{-2} at 254 nm wavelength at the sample position (measured with Thorlabs S120VC power sensor) degrades PMMA while cross-linking PS.[38] Additional UV exposure of up to 25 min was performed in the same chamber under constant nitrogen purging to further cross-link the PS features, resulting in a total dosage of 2 to 18 J cm^{-2}. The dosage on the samples was controlled by either varying the UV exposure time or by using a shadow mask. These exposed patterns were then subjected to thermal reflow on a preheated hotplate over a range of temperatures (95−125 °C) for up to 100 s. Patterning by electron-beam exposure was carried out in a JEOL JBX-6300FS electron-beam lithography tool at 100 kV using 1 nA beam current with exposure dosage in the range varying from 100 to 3000 μC/cm^2. Additional exposure tests were performed using a Nanometer Pattern Generation System on a Helios Nanolab (FEI) with exposure doses from 10−1000 μC/cm^2 at voltages from 1 to 10 kV.

Pattern Transfer. The patterns were transferred into Si substrates using either the remnant PS features as etch masks or the inverted patterns obtained from Al liftoff. The inverted patterns were obtained by thermal evaporation of ∼7.5 nm of Al (Kurt J. Lesker PVD 75) followed by liftoff using ultrasonication in warm toluene (40 °C) for 2 h. Transfer of the patterns (from etch masks formed by either inverted Al or the PS features) into Si substrates was then performed by RIE using a 40:18 combination of SF_6 and O_2 gas for 5−10 s at −100 °C (12 mTorr, 15−25 W RF power, 800 W ICP power). An initial 5 s high power etch step (40 W RF power and 800 W ICP power) was included for breakthrough and to strike the plasma. The samples etched with the PS etch mask were then cleaned with O_2 plasma (for 150 s at 21 W, 100 mTorr; March RIE) before further characterization. We note that the Al etch mask undergoes a small amount of depletion during the RIE process; however, a thin layer of ∼5 nm Al remains intact on top of the Si cylinders. Pattern transfer of the electron beam-exposed PS grating nanopatterns into Si was performed by RIE using a 44:11 combination of Cl_2 and O_2 gas for 60 s (10 mTorr, 40 W RF power, 250 W ICP power). An initial 6 s high power etch step (10 mTorr, 100 W RF power and 800 W ICP power) using a 20:5 combination of BCl_3 and Cl_2 gas was included to break through the native SiO_2.

Materials Characterization. Samples were imaged using a scanning electron microscope (Hitachi S-4800) at 10 kV, and the features were analyzed using ImageJ. The normal incidence reflectance measurements were carried out using Filmetrics F20-UV with a spot size of ∼500 μm in diameter. The bright-field photographs of the structural color samples were imaged using an Apple iPhone 12 Pro camera with an external normal incidence white LED source (AmScope LED−64S).

Cross-Linking Characterization. PS (22.0 kg/mol) films with a thickness of 198 ± 4 nm were obtained by spin coating from a 5% (w/w) solution in toluene onto O_2 plasma-cleaned silicon. Samples were then exposed to UV irradiation under constant nitrogen purging in the chamber described previously for times from 0 to 70 min in 14 min intervals. These samples were then placed together in the apparatus used for SVA described in ref 31, with 4 mL of tetrahydrofuran dispensed into an annular reservoir surrounding the samples. Sample thicknesses were measured in situ by visible-range spectral reflectance (Filmetrics F20-UV) prior to swelling and after a stable swollen film thickness was obtained (∼1 h). A Peltier plate was used to maintain a constant chamber temperature of 21.0 ± 0.2 °C, and no nitrogen purging was used during swelling measurements. The ratio of swollen film thickness to initial film thickness is plotted against the exposure time in Figure S3 of the Supporting Information. The swollen film thickness for unexposed PS could not be measured as the film fully dewetted during the experiment. Static water contact angles were measured on separate samples exposed to UV for the same intervals using an Ossila contact angle goniometer with manually dispensed 15 μL drops.

Optical Simulations. The normal incidence reflectance spectra of the transferred grating and pillar structures were simulated with Ansys-Lumerical Inc. FDTD (Release: 2020a r7, Version: 8.23.2347). Each optical response was obtained using a cross-polarized normal incident plane wave source and by applying periodic boundary conditions to the repeating structure. All nanopatterns were placed on a Si substrate extended through a perfectly matched layer boundary condition. The simulations in Figure 3 include the following parameters for gratings: straight lines of Si with 75 nm linewidth, 180 nm period, and 180 nm height with a vertical profile, and for pillars: triangular arrangement of Si pillars of 115 nm diameter, 210 nm period, 220 nm height with a vertical profile, and a 5 nm coating of Al on top of the pillars. The simulations for the etched pillars in Figure 4 include triangular arrangement of Si pillars of 95, 100, and 110 nm diameter, 210 nm period, 270 nm height with a vertical profile, and a 5 nm coating of Al on top of the pillars. The simulations for etched gratings in Figure 5 include straight lines of Si with 70 and 100 nm linewidth, 180 nm period, and 205 nm height with a vertical profile. The simulations for etched gratings in Figure S11 include straight lines of Si with 70, 80, 95, and 100 nm linewidth, 180 nm period, and 320 nm height with a vertical profile. The simulations for etched gratings in Figure S12 include straight lines of Si with 180, 190, 200, and 205 nm heights with a vertical profile, 70 nm linewidth, and 180 nm period.

ASSOCIATED CONTENT

Supporting Information

The Supporting Information is available free of charge at https://pubs.acs.org/doi/10.1021/acsami.2c05911.

Data and SEM images corresponding to solvent vapor annealing conditions; a plot of swollen film thickness ratio under tetrahydrofuran vapor vs UV exposure time; plots of feature size for varying reflow conditions and UV exposure times; SEM images of grating and hole patterns exposed to various exposure and reflow conditions; SEM images and schematics of transferred patterns; fast Fourier transforms of selected SEM images from samples after reflow and RIE into silicon; experimental and simulated reflectance spectra for silicon grating patterns with varying linewidths and heights (PDF)

AUTHOR INFORMATION

Corresponding Author

Gregory S. Doerk − *Center for Functional Nanomaterials, Brookhaven National Laboratory, Upton, New York 11973, United States*; orcid.org/0000-0002-2933-2047; Email: gdoerk@bnl.gov

Author

Ashish A. Kulkarni − *Center for Functional Nanomaterials, Brookhaven National Laboratory, Upton, New York 11973, United States*; orcid.org/0000-0003-0268-9756

Complete contact information is available at: https://pubs.acs.org/10.1021/acsami.2c05911

Author Contributions

A.A.K. and G.S.D. prepared samples, performed measurements, and analyzed results. The manuscript was written through contributions of all authors. All authors have given approval to the final version of the manuscript.

Notes

The authors declare no competing financial interest.

ACKNOWLEDGMENTS

This research used the Materials Synthesis and Characterization Facility and Nanofabrication Facility at the Center for Functional Nanomaterials (CFN), which is a U.S. Department of Energy Office of Science User Facility, at Brookhaven National Laboratory under Contract No. DE-SC0012704. G.S.D. acknowledges Dr. Sebastian Russell for helpful suggestions on the characterization of cross-linking behavior.

REFERENCES

(1) Arbabi, A.; Horie, Y.; Bagheri, M.; Faraon, A. Dielectric Metasurfaces for Complete Control of Phase and Polarization with Subwavelength Spatial Resolution and High Transmission. *Nat. Nanotechnol.* **2015**, *10*, 937−943.

(2) Yang, W.; Xiao, S.; Song, Q.; Liu, Y.; Wu, Y.; Wang, S.; Yu, J.; Han, J.; Tsai, D.-P. All-Dielectric Metasurface for High-Performance Structural Color. *Nat. Commun.* **2020**, *11*, 1864.

(3) Tan, S. J.; Zhang, L.; Zhu, D.; Goh, X. M.; Wang, Y. M.; Kumar, K.; Qiu, C.-W.; Yang, J. K. W. Plasmonic Color Palettes for Photorealistic Printing with Aluminum Nanostructures. *Nano Lett.* **2014**, *14*, 4023−4029.

(4) Yu, N.; Capasso, F. Flat Optics with Designer Metasurfaces. *Nat. Mater.* **2014**, *13*, 139−150.

(5) Holsteen, A. L.; Cihan, A. F.; Brongersma, M. L. Temporal Color Mixing and Dynamic Beam Shaping with Silicon Metasurfaces. *Science* **2019**, *365*, 257−260.

(6) Kim, I.; Yoon, G.; Jang, J.; Genevet, P.; Nam, K. T.; Rho, J. Outfitting Next Generation Displays with Optical Metasurfaces. *ACS Photonics* **2018**, *5*, 3876−3895.

(7) Zhu, X.; Vannahme, C.; Højlund-Nielsen, E.; Mortensen, N. A.; Kristensen, A. Plasmonic Colour Laser Printing. *Nat. Nanotechnol.* **2016**, *11*, 325−329.

(8) Bezares, F. J.; Long, J. P.; Glembocki, O. J.; Guo, J.; Rendell, R. W.; Kasica, R.; Shirey, L.; Owrutsky, J. C.; Caldwell, J. D. Mie Resonance-Enhanced Light Absorption in Periodic Silicon Nanopillar Arrays. *Opt. Express* **2013**, *21*, 27587.

(9) Park, J.-S.; Zhang, S.; She, A.; Chen, W. T.; Lin, P.; Yousef, K. M. A.; Cheng, J.-X.; Capasso, F. All-Glass, Large Metalens at Visible Wavelength Using Deep-Ultraviolet Projection Lithography. *Nano Lett.* **2019**, *19*, 8673−8682.

(10) Hu, T.; Tseng, C.-K.; Fu, Y. H.; Xu, Z.; Dong, Y.; Wang, S.; Lai, K. H.; Bliznetsov, V.; Zhu, S.; Lin, Q.; Gu, Y. Demonstration of Color Display Metasurfaces via Immersion Lithography on a 12-Inch Silicon Wafer. *Opt. Express* **2018**, *26*, 19548−19554.

(11) Moon, S.-W.; Kim, Y.; Yoon, G.; Rho, J. Recent Progress on Ultrathin Metalenses for Flat Optics. *iScience* **2020**, *23*, No. 101877.

(12) Yoon, G.; Kim, K.; Huh, D.; Lee, H.; Rho, J. Single-Step Manufacturing of Hierarchical Dielectric Metalens in the Visible. *Nat. Commun.* **2020**, *11*, 2268.

(13) Einck, V. J.; Torfeh, M.; McClung, A.; Jung, D. E.; Mansouree, M.; Arbabi, A.; Watkins, J. J. Scalable Nanoimprint Lithography Process for Manufacturing Visible Metasurfaces Composed of High Aspect Ratio TiO_2 Meta-Atoms. *ACS Photonics* **2021**, *8*, 2400−2409.

(14) Sreenivasan, S. V. Nanoimprint Lithography Steppers for Volume Fabrication of Leading-Edge Semiconductor Integrated Circuits. *Microsyst. Nanoeng.* **2017**, *3*, 1−19.

(15) Neshev, D.; Aharonovich, I. Optical Metasurfaces: New Generation Building Blocks for Multi-Functional Optics. *Light: Sci. Appl.* **2018**, *7*, 58.

(16) Siddique, R. H.; Mertens, J.; Hölscher, H.; Vignolini, S. Scalable and Controlled Self-Assembly of Aluminum-Based Random Plasmonic Metasurfaces. *Light: Sci. Appl.* **2017**, *6*, e17015−e17015.

(17) Zheng, H.; Zhou, Y.; Ugwu, C. F.; Du, A.; Kravchenko, I. I.; Valentine, J. G. Large-Scale Metasurfaces Based on Grayscale Nanosphere Lithography. *ACS Photonics* **2021**, *8*, 1824−1831.

(18) McLeod, E.; Ozcan, A. Nano-Imaging Enabled via Self-Assembly. *Nano Today* **2014**, *9*, 560−573.

(19) Singh, G.; Batra, S.; Zhang, R.; Yuan, H.; Yager, K. G.; Cakmak, M.; Berry, B.; Karim, A. Large-Scale Roll-to-Roll Fabrication of Vertically Oriented Block Copolymer Thin Films. *ACS Nano* **2013**, *7*, 5291−5299.

(20) Liu, C.-C.; Franke, E.; Mignot, Y.; Xie, R.; Yeung, C. W.; Zhang, J.; Chi, C.; Zhang, C.; Farrell, R.; Lai, K.; Tsai, H.; Felix, N.; Corliss, D. Directed Self-Assembly of Block Copolymers for 7 Nanometre FinFET Technology and Beyond. *Nat. Electron.* **2018**, *1*, 562−569.

(21) Stein, A.; Wright, G.; Yager, K. G.; Doerk, G. S.; Black, C. T. Selective Directed Self-Assembly of Coexisting Morphologies Using Block Copolymer Blends. *Nat. Commun.* **2016**, 12366−12366.

(22) Tavakkoli, K. G. A.; Gotrik, K. W.; Hannon, A. F.; Alexander-Katz, A.; Ross, C. A.; Berggren, K. K. Templating Three-Dimensional Self-Assembled Structures in Bilayer Block Copolymer Films. *Science* **2012**, *336*, 1294−1298.

(23) Tavakkoli, K. G. A.; Nicaise, S. M.; Hannon, A. F.; Gotrik, K. W.; Alexander-Katz, A.; Ross, C. A.; Berggren, K. K. Sacrificial-Post Templating Method for Block Copolymer Self-Assembly. *Small* **2014**, *10*, 493−499.

(24) Bosworth, J. K.; Black, C. T.; Ober, C. K. Selective Area Control of Self-Assembled Pattern Architecture Using a Lithographically Patternable Block Copolymer. *ACS Nano* **2009**, *3*, 1761−1766.

(25) Son, J. G.; Chang, J.-B.; Berggren, K. K.; Ross, C. A. Assembly of Sub-10-Nm Block Copolymer Patterns with Mixed Morphology and Period Using Electron Irradiation and Solvent Annealing. *Nano Lett.* **2011**, *11*, 5079−5084.

(26) Choi, C.; Park, J.; Vincent Joseph, K. L.; Lee, J.; Ahn, S.; Kwak, J.; Lee, K. S.; Kim, J. K. Simultaneous Fabrication of Line and Dot Dual Nanopatterns Using Miktoarm Block Copolymer with Photocleavable Linker. *Nat. Commun.* **2017**, *8*, 1765.

(27) Qiang, Z.; Akolawala, S. A.; Wang, M. Simultaneous In-Film Polymer Synthesis and Self-Assembly for Hierarchical Nanopatterns. *ACS Macro Lett.* **2018**, *7*, 566−571.

(28) Zhang, R.; Qiang, Z.; Wang, M. Integration of Polymer Synthesis and Self-Assembly for Controlled Periodicity and Photonic Properties. *Adv. Funct. Mater.* **2021**, *31*, No. 2005819.

(29) Zhang, W.; Sun, Z.; Jiang, Y.; Liu, X.; Gupta, R.; Russell, T. P.; Bryan Coughlin, E. Tuning Microdomain Spacing with Light Using Ortho-Nitrobenzyl-Linked Triblock Copolymers. *J. Polym. Sci., Part B: Polym. Phys.* **2018**, *56*, 355−361.

(30) Onses, M. S.; Song, C.; Williamson, L.; Sutanto, E.; Ferreira, P. M.; Alleyne, A. G.; Nealey, P. F.; Ahn, H.; Rogers, J. A. Hierarchical Patterns of Three-Dimensional Block-Copolymer Films Formed by Electrohydrodynamic Jet Printing and Self-Assembly. *Nat. Nanotechnol.* **2013**, *8*, 667−675.

(31) Doerk, G. S.; Li, R.; Fukuto, M.; Yager, K. G. Wet Brush Homopolymers as "Smart Solvents" for Rapid, Large Period Block Copolymer Thin Film Self-Assembly. *Macromolecules* **2020**, *53*, 1098−1113.

(32) Hong, S. W.; Gu, W.; Huh, J.; Sveinbjornsson, B. R.; Jeong, G.; Grubbs, R. H.; Russell, T. P. On the Self-Assembly of Brush Block Copolymers in Thin Films. *ACS Nano* **2013**, *7*, 9684−9692.

(33) Kim, E.; Ahn, H.; Park, S.; Lee, H.; Lee, M.; Lee, S.; Kim, T.; Kwak, E.-A.; Lee, J. H.; Lei, X.; Huh, J.; Bang, J.; Lee, B.; Ryu, D. Y. Directed Assembly of High Molecular Weight Block Copolymers: Highly Ordered Line Patterns of Perpendicularly Oriented Lamellae with Large Periods. *ACS Nano* **2013**, *7*, 1952−1960.

(34) Gorzolnik, B.; Mela, P.; Moeller, M. Nano-Structured Micropatterns by Combination of Block Copolymer Self-Assembly and UV Photolithography. *Nanotechnology* **2006**, *17*, 5027−5032.

(35) Hulkkonen, H.; Sah, A.; Niemi, T. All-Metal Broadband Optical Absorbers Based on Block Copolymer Nanolithography. *ACS Appl. Mater. Interfaces* **2018**, *10*, 42941−42947.

(36) Rahman, A.; Ashraf, A.; Xin, H.; Tong, X.; Sutter, P.; Eisaman, M. D.; Black, C. T. Sub-50-Nm Self-Assembled Nanotextures for Enhanced Broadband Antireflection in Silicon Solar Cells. *Nat. Commun.* **2015**, *6*, 5963.

(37) Kulkarni, A. A.; Doerk, G. Thin Film Block Copolymer Self-Assembly for Nanophotonics. *Nanotechnology* **2022**, *29*, 292001.

(38) Thurn-Albrecht, T.; Steiner, R.; DeRouchey, J.; Stafford, C. M.; Huang, E.; Bal, M.; Tuominen, M.; Hawker, C. J.; Russell, T. P. Nanoscopic Templates from Oriented Block Copolymer Films. *Adv. Mater.* **2000**, *12*, 787−791.

(39) Torres, J. M.; Stafford, C. M.; Vogt, B. D. Manipulation of the Elastic Modulus of Polymers at the Nanoscale: Influence of UV−Ozone Cross-Linking and Plasticizer. *ACS Nano* **2010**, *4*, 5357−5365.

(40) Yu, X.; Beharaj, A.; Grinstaff, M. W.; Tsui, O. K. C. Modulation of the Effective Viscosity of Polymer Films by Ultraviolet Ozone Treatment. *Polymer* **2017**, *116*, 498−505.

(41) Li, L.; Zhong, Y.; Li, J.; Chen, C.; Zhang, A.; Xu, J.; Ma, Z. Thermally Stable and Solvent Resistant Honeycomb Structured Polystyrene Films via Photochemical Cross-Linking. *J. Mater. Chem.* **2009**, *19*, 7222−7227.

(42) Palacios, M.; García, O.; Rodríguez-Hernández, J. Constructing Robust and Functional Micropatterns on Polystyrene Surfaces by Using Deep UV Irradiation. *Langmuir* **2013**, *29*, 2756−2763.

(43) Rabek, J. F.; Rånby, B. Studies on the Photooxidation Mechanism of Polymers. I. Photolysis and Photooxidation of Polystyrene. *J. Polym. Sci., Polym. Chem. Ed.* **1974**, *12*, 273−294.

(44) Kizilkaya, O.; Ono, M.; Morikawa, E. Characterization of the Photo-Irradiation Effects on Polystyrene Ultrathin Films with Ultraviolet Photoemission Spectroscopy. *J. Electron Spectrosc. Relat. Phenom.* **2006**, *151*, 34−39.

(45) Wells, R. K.; Royston, A.; Badyal, J. P. S. Direct Evidence for the Generation of Phenyl Radicals and Crosslinking during the Photolysis of a Polystyrene Film. *Macromolecules* **1994**, *27*, 7465−7468.

(46) Flory, P. J.; Rehner, J. Statistical Mechanics of Cross-Linked Polymer Networks II Swelling. *J. Chem. Phys.* **1943**, *11*, 521−526.

(47) Callen, B. W.; Ridge, M. L.; Lahooti, S.; Neumann, A. W.; Sodhi, R. N. S. Remote Plasma and Ultraviolet−Ozone Modification of Polystyrene. *J. Vac. Sci. Technol., A* **1995**, *13*, 2023−2029.

(48) Klein, R. J.; Fischer, D. A.; Lenhart, J. L. Systematic Oxidation of Polystyrene by Ultraviolet-Ozone, Characterized by Near-Edge X-Ray Absorption Fine Structure and Contact Angle. *Langmuir* **2008**, *24*, 8187−8197.

(49) Gharbi, A.; Tiron, R.; Pimenta Barros, P.; Argoud, M.; Servin, I.; Chevalier, X.; Nicolet, C.; Navarro, C. PMMA Removal Options by Wet Development in PS-b-PMMA Block Copolymer for Nanolitho-

graphic Mask Fabrication. *J. Vac. Sci. Technol., B* **2015**, *33*, No. 051602.
(50) Zhou, Z.; Li, J.; Su, R.; Yao, B.; Fang, H.; Li, K.; Zhou, L.; Liu, J.; Stellinga, D.; Reardon, C. P.; Krauss, T. F.; Wang, X. Efficient Silicon Metasurfaces for Visible Light. *ACS Photonics* **2017**, *4*, 544−551.
(51) Gokan, H.; Esho, S.; Ohnishi, Y. Dry Etch Resistance of Organic Materials. *J. Electrochem. Soc.* **1983**, *130*, 143.
(52) Oehrlein, G. S.; Phaneuf, R. J.; Graves, D. B. Plasma-Polymer Interactions: A Review of Progress in Understanding Polymer Resist Mask Durability during Plasma Etching for Nanoscale Fabrication. *J. Vac. Sci. Technol., B* **2011**, *29*, No. 010801.
(53) Yue, W.; Gao, S.; Lee, S.-S.; Kim, E.-S.; Choi, D.-Y. Subtractive Color Filters Based on a Silicon-Aluminum Hybrid-Nanodisk Metasurface Enabling Enhanced Color Purity. *Sci. Rep.* **2016**, *6*, 29756.
(54) Doerk, G. S.; Yager, K. G. Rapid Ordering in "Wet Brush" Block Copolymer/Homopolymer Ternary Blends. *ACS Nano* **2017**, *11*, 12326−12336.
(55) Doerk, G. S.; Cheng, J. Y.; Singh, G.; Rettner, C. T.; Pitera, J. W.; Balakrishnan, S.; Arellano, N.; Sanders, D. P. Enabling Complex Nanoscale Pattern Customization Using Directed Self-Assembly. *Nat. Commun.* **2014**, *5*, 5805−5805.
(56) Majewski, P. W.; Rahman, A.; Black, C. T.; Yager, K. G. Arbitrary Lattice Symmetries via Block Copolymer Nanomeshes. *Nat. Commun.* **2015**, *6*, 7448−7448.
(57) Ruiz, R.; Kang, H.; Detcheverry, F. A.; Dobisz, E.; Kercher, D. S.; Albrecht, T. R.; de Pablo, J. J.; Nealey, P. F. Density Multiplication and Improved Lithography by Directed Block Copolymer Assembly. *Science* **2008**, *321*, 936−939.
(58) Doerk, G. S.; Liu, C.-C.; Cheng, J. Y.; Rettner, C. T.; Pitera, J. W.; Krupp, L. E.; Topuria, T.; Arellano, N.; Sanders, D. P. Pattern Placement Accuracy in Block Copolymer Directed Self-Assembly Based on Chemical Epitaxy. *ACS Nano* **2013**, *7*, 276−285.
(59) Jang, J.; Badloe, T.; Yang, Y.; Lee, T.; Mun, J.; Rho, J. Spectral Modulation through the Hybridization of Mie-Scatterers and Quasi-Guided Mode Resonances: Realizing Full and Gradients of Structural Color. *ACS Nano* **2020**, *14*, 15317−15326.
(60) Lee, T.; Kim, J.; Koirala, I.; Yang, Y.; Badloe, T.; Jang, J.; Rho, J. Nearly Perfect Transmissive Subtractive Coloration through the Spectral Amplification of Mie Scattering and Lattice Resonance. *ACS Appl. Mater. Interfaces* **2021**, *13*, 26299−26307.
(61) Kuznetsov, A. I.; Miroshnichenko, A. E.; Brongersma, M. L.; Kivshar, Y. S.; Luk'yanchuk, B. Optically Resonant Dielectric Nanostructures. *Science* **2016**, *354*, No. aag2472.
(62) Ma, S.; Con, C.; Yavuz, M.; Cui, B. Polystyrene Negative Resist for High-Resolution Electron Beam Lithography. *Nanoscale Res. Lett.* **2011**, *6*, 446.
(63) Lee, H. M.; Kim, Y. N.; Kim, B. H.; Kim, S. O.; Cho, S. O. Fabrication of Luminescent Nanoarchitectures by Electron Irradiation of Polystyrene. *Adv. Mater.* **2008**, *20*, 2094−2098.
(64) Bhuvana, T.; Kulkarni, G. U. Polystyrene as a Zwitter Resist in Electron Beam Lithography Based Electroless Patterning of Gold. *Bull. Mater. Sci.* **2008**, *31*, 201−206.
(65) Qu, C.; Kinzel, E. C. Polycrystalline Metasurface Perfect Absorbers Fabricated Using Microsphere Photolithography. *Opt. Lett.* **2016**, *41*, 3399−3402.
(66) Moitra, P.; Slovick, B. A.; Li, W.; Kravchencko, I. I.; Briggs, D. P.; Krishnamurthy, S.; Valentine, J. Large-Scale All-Dielectric Metamaterial Perfect Reflectors. *ACS Photonics* **2015**, *2*, 692−698.
(67) Yokogawa, S.; Burgos, S. P.; Atwater, H. A. Plasmonic Color Filters for CMOS Image Sensor Applications. *Nano Lett.* **2012**, *12*, 4349−4354.
(68) Subramanian, A.; Doerk, G.; Kisslinger, K.; Yi, D. H.; Grubbs, R. B.; Nam, C.-Y. Three-Dimensional Electroactive ZnO Nanomesh Directly Derived from Hierarchically Self-Assembled Block Copolymer Thin Films. *Nanoscale* **2019**, *11*, 9533−9546.
(69) Subramanian, A.; Tiwale, N.; Doerk, G.; Kisslinger, K.; Nam, C.-Y. Enhanced Hybridization and Nanopatterning via Heated Liquid-Phase Infiltration into Self-Assembled Block Copolymer Thin Films. *ACS Appl. Mater. Interfaces* **2020**, *12*, 1444−1453.
(70) Ok, J. G.; Kwak, M. K.; Huard, C. M.; Youn, H. S.; Guo, L. J. Photo−Roll Lithography (PRL) for Continuous and Scalable Patterning with Application in Flexible Electronics. *Adv. Mater.* **2013**, *25*, 6554−6561.

Recommended by ACS

Photoinduced Alignment under Solvent Vapor Annealing (PA-SVA): Enhanced Ordering and Patterning in Block Copolymer Films

Yu-Hsuan Tseng, Jiun-Tai Chen, *et al.*

NOVEMBER 01, 2022
ACS APPLIED POLYMER MATERIALS
READ

Highly Ordered Porous Inorganic Structures *via* Block Copolymer Lithography: An Application of the Versatile and Selective Infiltration of the "Inverse" P2VP-*b*-PS System

Aislan Esmeraldo Paiva, Michael Morris, *et al.*

JULY 25, 2022
ACS APPLIED MATERIALS & INTERFACES
READ

Layered Thin Film Deposition via Extreme Inter-Brush Slip in a Lamellar Block Copolymer

Wenpeng Shan, Edwin L. Thomas, *et al.*

OCTOBER 05, 2022
MACROMOLECULES
READ

Vacuum-Driven Orientation of Nanostructured Diblock Copolymer Thin Films

Aum Sagar Panda, Rong-Ming Ho, *et al.*

JULY 29, 2022
ACS NANO
READ

Get More Suggestions >

https://doi.org/10.1021/acsami.2c05911
ACS Appl. Mater. Interfaces 2022, 14, 27466−27475